Toxicology Letters 383 (2023) 128–140

Contents lists available at ScienceDirect

Toxicology Letters

journal homepage: www.journals.elsevier.com/toxicology-letters

Development of a rat physiologically based kinetic model (PBK) for three organophosphate flame retardants (TDCIPP, TCIPP, TCEP)

Deepika Deepika [a], Raju Prasad Sharma [a], Marta Schuhmacher [a], Vikas Kumar [a,b,*]

[a] Environmental Engineering Laboratory, Departament d' Enginyeria Quimica, Universitat Rovira i Virgili, Av. Països Catalans 26, 43007, Tarragona, Catalonia, Spain
[b] IISPV, Hospital Universitari Sant Joan de Reus, Universitat Rovira I Virgili, Reus, Spain

ARTICLE INFO

Editor: Dr. Angela Mally

Keywords:
PBK model
Organophosphate flame retardants
Tris(1,3-dichloro-2-propyl), phosphate (TDCIPP)
Tris (1-chloro-2-propyl) phosphate (TCIPP)
Tris (2-chloroethyl), phosphate (TCEP)
Enterohepatic Recirculation (EHR)
PBK-IVIVE
Neurotoxicity
Human Health risk assessment

ABSTRACT

Tris(1,3-dichloro-2-propyl) phosphate (TDCIPP), Tris (1-chloro-2-propyl) phosphate (TCIPP) and tris (2-chloroethyl) phosphate (TCEP) are three widely used organophosphate flame retardants (OPFRs) being frequently detected in human body fluids. Although OPFRs are being detected in human beings, the toxicological effects of their exposure are not clearly understood due to limited data. For this, a physiologically based kinetic model (PBK) was developed in MCSIM integrated with R studio and validated in rats to understand the toxicokinetics of OPFRs for the first time. The model required the enterohepatic recirculation (EHR) mechanism which was included to explain the non-linear data. Model parameters were optimized using the Bayesian framework (Markov Chain Monte Carlo) along with a visual fitting to explain toxicokinetic data. Goodness-of-fit was calculated to evaluate model predictability power in Rstudio. The model can appropriately predict the concentration of OPFRs in several organs like plasma, urine, kidney, etc. within 1–2-fold of experimental data. Slow elimination of OPFRs was observed from adipose tissue and brain at late time points, showing their potential to accumulate upon daily exposure. The use of PBK was demonstrated by reconstructing the oral exposure equivalent to the in-vitro toxic dose to support neurotoxic risk assessment. This version of PBK can be extrapolated to human for toxicological risk assessment. Nonetheless, further investigation is required to understand whether these chemicals follow similar kinetics in humans, which could lead to a greater risk to human health. *Code availability:* The model will be available to access through Rshiny using GITHub soon, InSilicoVida/Flame-Retardant-PBPK-Model: It contains organophosphate flame retardant (OPFRs) PBK for TDCIPP, TCIPP and TCEP (github.com).

1. Introduction

Organophosphate flame retardants (OPFRs) contain an alkyl chain or aryl polymer group with an organic ester of phosphoric acid with or without a halogen group and can be either reactive or additive depending on the addition of reactive components or mixing into another polymer (Huang et al., 2022). They are also phosphites oxidation product and are used in manufacturing of plastic products. Recently their use has increased as plasticizers in construction and for the fire safety standard (Blum et al., 2019). The reason being other flame retardant like PBDE (Polybrominated Diethyl Ether) has been phased out of the USA and banned in Europe due to human health concerns (Hogberg et al., 2021). That's why, OPFRs are the second most widely used FR (Flame Retardant) in Europe after aluminium trihydroxide with an approximate consumption of 89640 metric tons almost double of BFRs (Chupeau et al., 2020).

Several studies showed OPFRs associated with various adversity such as neurotoxicity, endocrine disruption, carcinogenicity, and developmental toxicity (Hoffman et al., 2014; Yang et al., 2019, 2022; Yao et al., 2021). Humans are exposed to OPFRs through dietary intake, inhalation, dermal contact and ingestion of indoor dust (Hou et al., 2016; Wang et al., 2020a). Dust ingestion is considered a major contributor for exposure with ingestion estimated to be 6.6 ng/Kg BW/d for nonworking adults and 128 ng/Kg BW/d for children in Belgium (Chupeau et al., 2020). In general, exposure levels of OPFRs are found to be higher in children than adults and also levels are continuously increasing in indoor air and dust samples (Esplugas et al., 2022). OPFRs are frequently used as additives rather than chemically bonded to materials, as a result, they are easily released to different environmental matrices via volatilization, leaching and/or abrasion (van den Eede

* Correspondence to: Environmental Engineering Laboratory, Departament d.625*pt*'Enginyeria Química, Universitat Rovira i Virgili, Tarragona, Catalonia, Spain.
E-mail address: vikas.kumar@urv.cat (V. Kumar).

https://doi.org/10.1016/j.toxlet.2023.06.006
Received 30 December 2022; Received in revised form 14 June 2023; Accepted 20 June 2023
Available online 24 June 2023

et al., 2016). Numerous studies detected OPFRs in both indoor and outdoor environments (dust, furniture and ambient air) (Bajard et al., 2019; Esplugas et al., 2022; Zhang et al., 2016). A study conducted in Sweden suggested phosphorus flame retardants (PFR), daily per capita intake from food ranges from 406 to 3266 ng/day equivalent to 6–49 ng/Kg BW/day (Poma et al., 2017). This result suggested human dietary intake of PFR is equally important to dust ingestion. Further in recent years, European Commission banned the use of organohalogen chemicals in electronic displays and stands (Schreder, 2019) which forced the manufacturers to explore the potential of using OPFRs as a replacement substitute. As a result, the use of OPFRs is continuously increasing and being a persistent organic pollutant, it bioaccumulates (Hou et al., 2016).

Human biomonitoring studies detected OPFRs and their metabolites in various biological samples such as blood, urine, (Wang et al., 2020b) hair and milk (Chupeau et al., 2020). OPFRs are ubiquitous in the environment and increasingly raised health concerns (Yao et al., 2021), making it crucial to understand their toxicokinetic in living beings. As per our knowledge, currently, there is no PBK Model developed to understand their disposition. Also, there is sparse data regarding the dynamics and kinetics of OPFRs. There are few experimental data available with kinetic studies in rats and mice (Lynn et al., 1981; Minegishi et al., 1988; Nomeir et al., 1981; Zhu et al., 2020). For instance, Minegishi et al., compared the PK of several OPFRs in rats after exposure through oral route (Minegishi et al., 1988). The study by Lynn et al. and Chapman et al. reported TDCIPP disposition in rats after IV exposure (Chapman et al., 1991; Lynn et al., 1981). In general, for OPFRs, almost all parent compounds get metabolized quickly to the metabolites, but their elimination is relatively slow in living beings (Lynn et al., 1981; Nomeir et al., 1981). Nomeir et al. conducted a biliary excretion study and pointed out that radioactive TDCIPP was excreted in bile within 4 h while the feces excretion was over the course of 10 days (Nomeir et al., 1981). This indicates that the compound excreted in bile undergoes enterohepatic recirculation (EHR). Such kind of phenomenon can be captured through the PBK model by integrating in-vitro metabolism data, and available mechanistic evidence along with physiology, biochemical and physicochemical properties (McNally et al., 2021).

The objective of this work was to develop and validate the PBK model for three OPFRs in rats to understand the biology influencing the distribution of these compounds in organs like brain, adipose tissue, liver etc. To achieve this objective, a perfusion-limited PBK model was developed for understanding the toxicokinetic inside a living being. *In vitro* data was scaled for rat through an in-vitro to in-vivo extrapolation (IVIVE) approach and used as input to develop the PBK model. Sensitivity analysis was conducted to find the physiological and biochemical parameters affecting the output. Further, the application of developed model was demonstrated using dosimetry IVIVE for neurotoxicity risk assessment. The developed PBK model can be used further for the human risk assessment by cross-species extrapolation. This model has been developed for data-deficient chemicals and can help in pointing out the existing gaps in the data of OPFRs which can be fulfilled by further experimental studies including targeted in-vitro studies.

2. Methodology

2.1. Building of the PBK model

A PBK model was developed comprising of the seven compartments

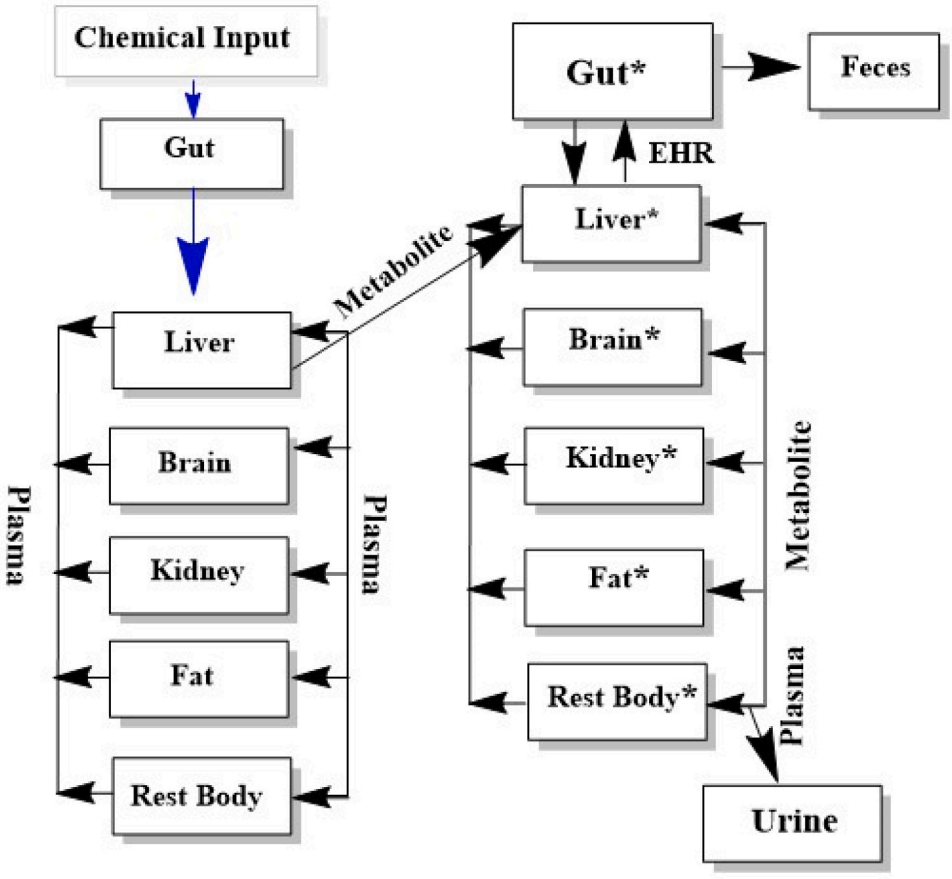

Fig. 1. PBK Model for three OPFRs with seven compartments. Enterohepatic recirculation (EHR) of the metabolite was included in the model. * represents the respective metabolite getting circulated inside human body. Metabolite is getting excreted from feces through gut and from urine through plasma. Almost all the parent compound is getting metabolized to metabolites.

i.e., gut, liver, brain, kidney, fat, plasma and the rest of the body along with their major metabolites: TDCIPP to bis(1,3-dichloro-2-propyl) phosphate (BDCIPP), TCIPP to bis(1-chloropropyl) phosphate (BCIPP) and TCEP to bis(2-chloroethyl) hydrogen phosphate (BCEP) respectively (Fig. 1 and Fig. 2). Chemical exchange between the organs and plasma is restricted by flow rather than permeation also called perfusion-limited model. The fundamental Eq. (1) used for developing PBK applies to all the compartments except chemical-eliminating organs such as liver, kidney and gut which includes additional clearance equations. For more details about equations, see supplementary file 1.

$$\frac{dC_i}{dt} = \frac{Q_i * C_p - \frac{C_i}{Ki:p}}{V_i} \quad (1)$$

Here, C_i refers to the concentration in the particular compartment i (μg/L), Q_i represents blood flow in i_{th} compartment, C_p represents concentration in plasma, Ki:p denotes partition coefficient of i_{th} compartment in relation to plasma and V_i is the volume of the i_{th} compartment.

2.2. Assumptions for building PBK model

Since both the three compounds belong to the family of organophosphates, a generic structure of PBK was utilized along with other assumptions like:

- ✓ Almost all chemical getting metabolized to their respective metabolite within a very short span of time.
- ✓ Two parallel PBK models: one for compound and other for metabolite with similar compartments.
- ✓ Inclusion of enterohepatic recirculation (EHR) due to non-linear kinetics.
- ✓ Urinary elimination from plasma only for metabolite. The chemical is metabolizing very fast and hence parent compounds are not getting eliminated from urine or feces.

2.3. Parameterization of the model

Parameterization of the PBK model includes physiological and biochemical parameters for the rat. All physiological parameters related to organ volumes and blood flows to respective organs were adopted from several articles published by authors as shown in Table 1 (Supplementary file 1) (Brown et al., 1997; Merrill et al., 2003; Sharma et al., 2020). Some biochemical parameters were optimized based on data from Minegishi et al. (1988) while others were calculated based on the experimental data (Minegishi et al., 1988; van den Eede et al., 2013, 2016). Markov Chain Monte Carlo (MCMC) algorithm was used for optimization along with visual fitting for many parameters. Further optimization details have been mentioned in supplementary file 2.

Table 1
Biochemical parameters for TDCIPP, TCIPP and TCEP. Monte Carlo (MC) was done to capture uncertainty and log-normal (LN) was used for distributing the parameter. The log-normal distribution is represented by two parameters: 1) geometric mean (exponential of mean in log-space) and geometric standard deviation (exponential of SD in log-space strictly superior to 1) (Bois, 2009).

Parameters	Values (TDCIPP), Distribution	Values (TCIPP), Distribution	Values (TCEP), Distribution
BW (Kg)	0.15	0.15	0.15
MW (g/mol)[a]	430.9	327.6	285.5
Log P (octanol/water)[b]	3.65	2.59	1.43
Liver: Plasma[c]	0.30 (LN 1.1)[c]	0.38 (LN 1.1)[c]	0.45 (LN 1.1)
Brain: Plasma[o,c]	0.13 (LN 1.1)	0.9 (LN 1.1)[c]	0.702 (LN 1.1)
Kidney: Plasma[o,c]	1.31 (LN 1.1)	5.25 (LN 1.1)	6.31 (LN 1.1)[c]
Fat: Plasma[o,c]	0.794 (LN 1.1)[c]	0.8 (LN 1.1)	2.09 (LN 1.1)[c]
Absorption Rate Constant (kgut, hr^{-1})°	0.098 (LN 1.1)	0.083 (LN 1.1)	0.5 (LN 1.1)
Absorption Rate Constant[d] (kgut_1, hr^{-1})°	0.099 (LN 1.1)	0.5 (LN 1.1)	0.5 (LN 1.1)
Enterohepatic recirculation (EHR_1, hr^{-1})°	3.01 (LN 1.1)	0.8 (LN 1.1)	18.99 (LN 1.1)
Fraction unbound (Fu)°	0.001 (LN 1.1)	0.035 (LN 1.1)	0.010 (LN 1.1)
Fraction unbound for metabolite (fu_1)°	0.019 (LN 1.1)	0.015 (LN 1.1)	0.035 (LN 1.2)
Vmax_liver_c[e] (μmol/hr/Kg BW)°	1509.11	1509.11	1509.11
Km_liver (μM)[f]	96.1[a]	96.1[a]	96.1[a]
Clearance rate (Cl, hr^{-1})°	0.040 (LN 1.1)	0.18 (LN 1.1)	0.98 (LN 1.1)
Fecal elimination rate (kfeces_c, hr^{-1})°	0.045 (LN 1.1)	0.065 (LN 1.1)	-

Parameters were calculated based on data from Minegishi et al. (1988).
It was assumed that all parameters will follow a log-normal distribution with a fixed geometric standard deviation. MC simulation included 10,000 iterations with parameters defined by random sampling from probability distribution mentioned below.

[a] reference (Tris(1,3-dichloro-2-propyl)phosphate | C9H15Cl6O4P - PubChem (nih.gov), Tris(1-chloro-2-propyl) phosphate | C9H18Cl3O4P - PubChem (nih.gov), Tris(2-chloroethyl) phosphate | C6H12Cl3O4P - PubChem (nih.gov))

[b] reference (Tris(1,3-dichloro-2-propyl)phosphate | C9H15Cl6O4P - PubChem (nih.gov), Tris(1-chloro-2-propyl) phosphate | C9H18Cl3O4P - PubChem (nih.gov), Tris(2-chloroethyl) phosphate | C6H12Cl3O4P - PubChem (nih.gov)

[c] refers to parameters calculated, o refers to parameter optimized and o,c refers to some parameters calculated for specific chemical and other optimized for another chemical based on the data from Minegishi et al. (1988).

[d] Refers to absorption rate constant for metabolite.

[e] represents Vmax for major metabolite in liver assumed to be similar.

[f] The data for km_liver was extracted from van den Eede et al. (2013, 2016).

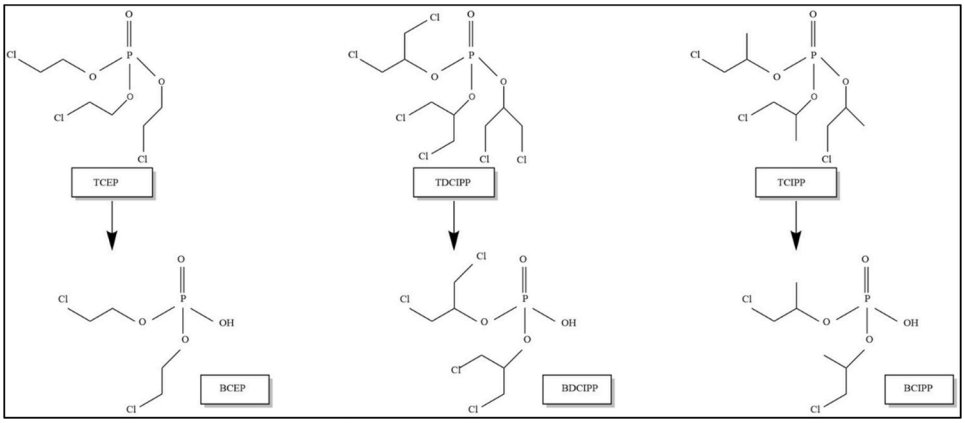

Fig. 2. Chemical Structure of parent compound and its metabolites being considered for the PBK Model, Tris(2-chloroethyl) phosphate (TCEP), Tris(1-chloro-2-propyl) phosphate (TCIPP), and Tris(1,3-dichloro-2-propyl) phosphate (or isopropyl) (TDCIPP). For this model, we considered that metabolism is only happening in liver and major metabolites being formed are: bis(2-chloroethyl) hydrogen phosphate (BCEP), bis(1,3-dichloro-2-propyl) phosphate (BDCIPP), and bis(1-chloropropyl) phosphate (BCIPP).

2.3.1. Absorption and enterohepatic recirculation

PBK was built for oral administration with the gut as a site of absorption. The input of the dose was in stomach and was being monitored by gastric emptying to gut. Absorption from gut to liver was defined by first-order rate constant (Table 1). The enterohepatic recirculation (EHR) (Fig S1) process was included based on kinetic data that showed the biliary excretion of OPFRs and slow elimination in urine (Nomeir et al., 1981). In the experimental data, a secondary peak was observed resulting in slow elimination from 20 h after dose administration (Nomeir et al., 1981). The EHR process was modelled considering the metabolite only and not including parent compounds since the OPFRs undergo a very fast metabolism. For instance, in the case of TDCIPP, within 5 min of dose administration, the metabolite started appearing in all the organs and after 30 min, the parent compound was not detected (Lynn et al., 1981). Uptake of the OPFR was done from gut to liver, in liver it undergoes metabolism. Metabolite from liver to gut was modeled as first-order uptake process where the metabolite was available for reabsorption. Data on the reabsorption rate and uptake has been provided in Table 1.

2.3.2. Distribution of the OPFRs

Biochemical parameters such as partition coefficient were calculated for specific OPFRs based on experimental study (Minegishi et al., 1988). To calculate the partition coefficient, first, the AUC of different organs and plasma was determined using the trapezoidal method. Then the partition coefficient for several organs was calculated using Eq. 2 where Ki:p refers to the partition coefficient of the organ with respect to plasma, and AUC is the area under the curve. A separate fraction unbound was considered for the chemical and its metabolite which was available for distribution, metabolism and excretion from the human body (Table 1).

$$Ki:p = \frac{AUC_{Organ(0:24hours)}}{AUC_{Plasma(0:24hours)}} \tag{2}$$

2.3.3. Metabolism and excretion

Metabolism was determined by the Michaelis-Menten equation with parameters like Vmax (maximum reaction velocity at the saturable substrate concentration) and Km (concentration at which reaction occurs at the half-maximum rate) given in Eq. 3. Vmax was scaled from pmol/min/mg protein to in-vivo per kg BW (Eq. 4). MPPGL refers to microsomal protein per gram of the liver, V_{liver} represents the volume of liver in L (Table 1 in supp file), and BW refers to body weight in Kg. Metabolic equations were included in separate compartments responsible for the metabolism of chemicals (Fig. 1). Almost similar chemical structure of three chemicals depicts that they might have a similar kind of metabolic profile (Fig. 2). All three were considered as possible substrates of glutathione S-transferases (GSTs) since GSTs react primarily with electrophilic functions or substituents in the molecule (van den Eede et al., 2013). For TCEP, in terms of relative abundance, BCEP was the major metabolite (van den Eede et al., 2013) in the human liver. BDCIPP diester was the major metabolite measured followed by glutathione conjugate in TDCIPP (van den Eede et al., 2013). However, in the case of TCIPP, TCIPP-M2 and BCIPP were the major metabolite (van den Eede et al., 2016, 2013). The major metabolite was considered for the model except for TCIPP we considered only BCIPP since in human biomonitoring studies, most researcher quantify BCIPP shown in Fig. 2 (Ingle et al., 2018). A study by van den Eede et al. (2016) where the author calculated Vmax and Km for TCIPP in human liver microsomes was taken. For the plasma, the value was found very low, so the major metabolite (BCIPP) was being formed in liver. A similar assumption was considered and due to the limited availability of data, a similar kind of distribution was assumed for the other 2 OPFRs (Table 1).

$$k_{Organ} = \frac{V_{\max} * C_{organ} * f_u}{k_m + C_{organ} * f_u} \tag{3}$$

$$V_{\max} = V_{\max} * MPPGG * V_{liver} / BW^{0.75} \tag{4}$$

Excretion was explained by a urinary and fecal route which accounts for the major elimination of all three chemicals. However, for TCEP only urinary elimination was considered since it accounts for 90% of excretion. Several parameters were optimized by MCMC Bayesian analysis for fitting the toxicokinetic due to a lack of experimental data. After initial optimization, convergence for the parameters was not so optimal, however, it narrowed down the range for optimization. Value from initial optimization was considered for further refinement of several parameters by visually fitting within the margin of errors of the dataset for increasing the model goodness of fit (U. S. Environmental Protection Agency, 2006). All biochemical parameters calculated and fitted were provided in Table 1.

2.4. Calibration and evaluation of PBK using experimental animal data

OPFRs kinetics study in rats performed by Minegishi et al. (1988) measured the chemical concentrations at 3, 6, 12, 24, 72, and 168 h after a single dose of 50 μmol/kg administered orally to the group of five rats for all three OPFRs. This data was used for estimating specific parameters by defining unknown parameter prior value (supplementary file 2) (Minegishi et al., 1988). Further, this data was used to check the prediction of the PBK model. The goodness of fit was plotted for each model by comparing the simulating and observed data from Minegishi et al. (1988). R (correlation coefficient) and p-value was calculated for every organ using the Pearson correlation coefficient (PCC).

The other two independent datasets by Lynn et al. and Nomeir et al. were not used for parameter estimation but rather solely to check the model performance. In Lynn et al. study an IV dose of ^{14}C-TDCPP (10.04 μCi, sp. act. 12.5 mCi/mmol) was administered and the distribution, metabolism and excretion in rats in all organs were measured at 0.08, 0.5, 8, 24, and 120 h (Lynn et al., 1981). Extracted data from this study was used to further validate the TDCIPP model. In another study for TDCIPP by Nomeir et al., 2 μmol/Kg dose (0.867 mg/kg) was administered through the oral route and chemical concentrations was measured in all organs till 10 days (Nomeir et al., 1981). Nomeir et al. has clearly stated that the absorption of TDCIPP is so rapid that after absorption from the dermal route or the gastrointestinal tract (GIT), the tissue distribution is similar to the IV dose except for lungs. Another point worth mentioning is that all the parent compound gets metabolized quickly to the metabolites. The author checked after administering by both oral and IV route and found the tissue/blood distribution to be same after 24 h (Nomeir et al., 1981). Further, he checked for dermal administration and tissue blood ratio was similar as anticipated by oral and IV. Considering this, we have kept administration route which is oral similar for all our simulations.

2.5. Sensitivity analysis

A normalized sensitivity analysis (SA) for both the input parameters and output was used to evaluate the impact of input parameters on the area under the curve (AUC_{0-t}) of the plasma concentration (Loccisano et al., 2013). AUC was used since OPFRs have longer half-lives and calculating AUC can give a better estimate of the sensitivity. A single parameter was changed to 2% of its original value while all others were kept constant to evaluate the influence on the output. SA was performed at the dose of 50 μmol/Kg BW. The following Eq. 5 was used to calculate the SA.

$$SA = \frac{(AUC_{increase} - AUC_{original}) / AUC_{original}}{(Param_{increase} - Param_{Original}) / Param_{Original}} \tag{5}$$

Here, AUC refers to area under curve and param refers to the physiological and biochemical parameters included in the analysis.

Global sensitivity analysis (GSA) was also performed through pksensi

package in R (Hsieh et al., 2020). We varied all the input parameters by 2% and computed the effect on plasma, liver, brain and kidney AUC. Heat-map was made to differentiate between influential and non-influential parameters with a cut-off value (more than 0.1, influential, less than 0.05 non-influential), further details and fig. in supplementary file 2.

2.6. Dosimetry IVIVE for risk assessment

IVIVE was used to convert the in-vitro concentration at which toxicity was observed to an external exposure level using the PBK model. TDCIPP induced apoptotic death in PC12 cell lines at 50 μM through MAPK pathway by activating CaMK2 phosphorylation (Li et al., 2017a). For TCIPP, no article was found with neurotoxicity in the in-vitro cell line. However, there was one article with neurodevelopmental effects in zebrafish for TCIPP and TCEP, but it was not considered (Li et al., 2019). Cytotoxicity was observed in PC12 cell lines for TDCIPP and TCEP along with alteration in gene level of GAP43, two tubulins, NF-H and CAMKII gene levels (Ta et al., 2014). Exposure from PC-12 cell lines was considered (Li et al., 2017a; Ta et al., 2014) and the PBK model with dosimetry IVIVE was utilized (Emond et al. 2021). The highest concentration at which in-vitro adverse effect observed was considered as the input parameter ($C_{max\ in\text{-}vitro}$) for the PBK model and PBK model was used to estimate an oral equivalent dose required to achieve peak brain concentration with dosimetry IVIVE (Emond et al., 2021). Further details about this can be found in the literature (Chou et al., 2020). The

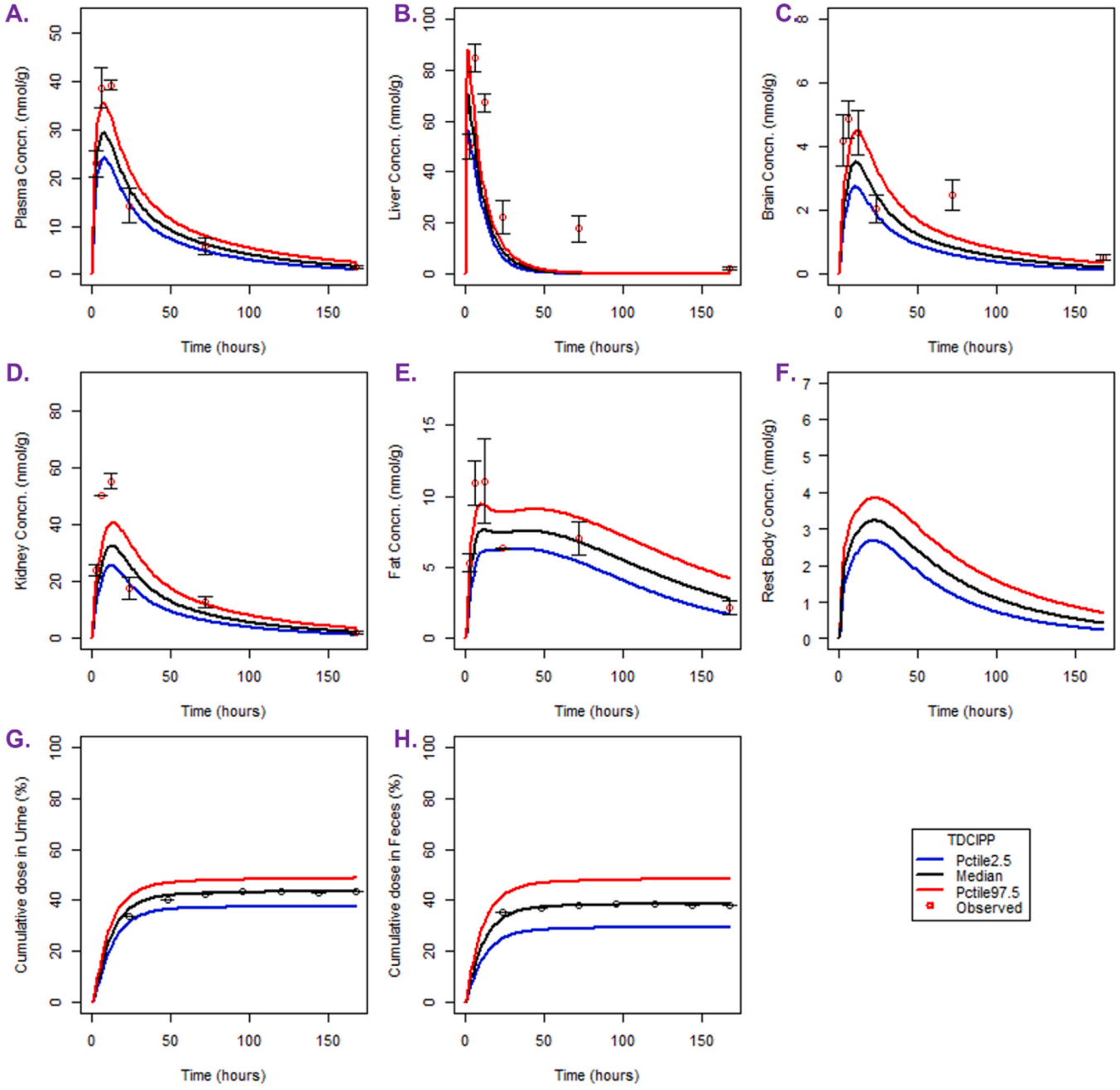

Fig. 3. Concentration-time curves for TDCIPP in plasma (A), liver (B), brain (C), kidney (D), fat (E), rest body (F), urine (G) and feces (H) at 50 μmol/Kg. The Y-axis showed the chemical concentrations (nmol/g) and cumulative dose excreted in urine and feces (%) and the X-axis showed the time in hrs. The solid lines correspond to the model simulation i.e., red (97.5th percentile), black (median), and blue (2.5th percentile), and the red dots (mean) with black bars (Standard deviations) represent the experimental value (Minegishi et al., 1988).

equation for calculating OED is

$$OED(mg/kg\ \ BW/day) = \frac{C_{\max,in-vitro}(\mu M) * 1(mg/Kg\ \ BW/day)}{C_{\max,ss}(\mu M)} \quad (6)$$

Here, $C_{max,in\text{-}vitro}$ is the maximum concentration at which in-vitro toxicity was observed (the input parameter), $C_{max,ss}$ is steady state brain concentration by PBK model after exposure to a daily dose of 1 mg/Kg BW/day.

Dosimetry risk assessment was done utilizing MCMC Simulation with 100,000 iterations consisting of four parallel chains. Initially, 25,000 iterations were burn-in (rejected) and the last 75,000 were considered as output iterations to ensure convergence. The output of each chain was inspected to assess the convergence. The Potential scale reduction factor (R) and Brooks-Gelman multivariate sink factor were calculated. The R value of less than 1.2 was considered as the threshold for convergence (Chou et al., 2020).

2.7. Computing software

Coding and simulation were performed with MCSIM (Bois, 2009) integrated with R studio (Version 4.1.2) (Team, 2015). For data analysis, Rstudio has been used with package like ggplot2, ggscatter, and ggpubr, for carrying out activities like plotting, correlation coefficient etc.

3. Results

3.1. Model evaluation for three OPFRs

The concentration-time plots were generated for three OPFRs in multiple organs upon oral administration of 50 μmol/Kg and the results were compared to the rat data published by Minegishi et al. (1988). Overall, the model predicted concentrations in different organs (liver, brain, kidney, fat, blood, urine and feces) were within 2–3 folds of the

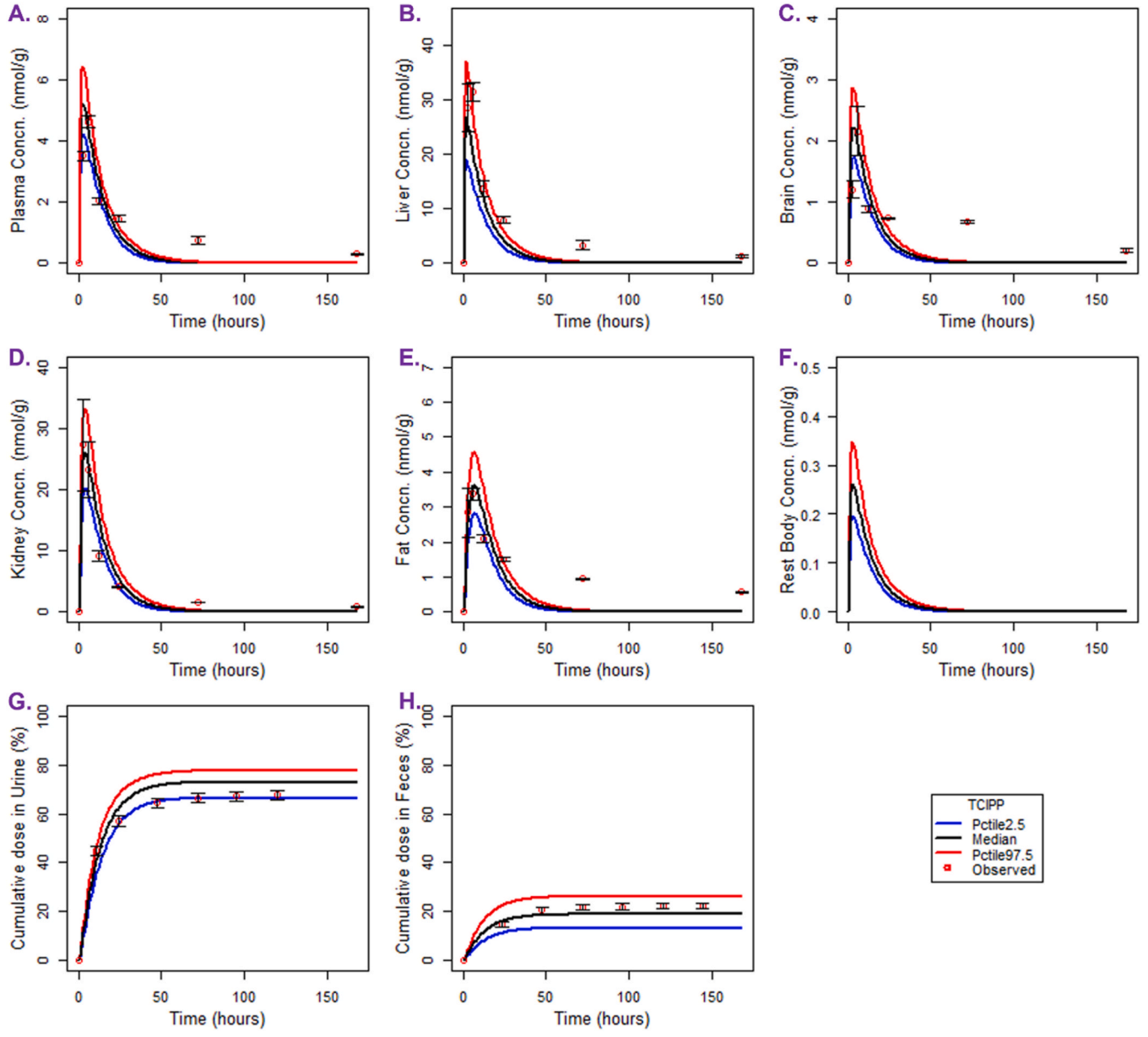

Fig. 4. Concentration-time curves for TCIPP in plasma (A), liver (B), brain (C), kidney (D), fat (E), rest body (F), urine (G) and feces (H) at 50 μmol/Kg. The Y-axis showed the chemical concentrations (nmol/g) and cumulative dose excreted in urine and feces (%) and the X-axis showed the time in hrs. The solid lines correspond to the model simulation i.e., red (97.5th percentile), black (median), and blue (2.5th percentile), and the red dots (mean) with black bars (Standard deviations) represent the experimental value (Minegishi et al., 1988).

experimental data. The model was able to predict very well the major elimination organ i.e., liver and kidney where the highest concentration was detected for all three OPFRs. At the same exposure level, the maximum plasma concentration (C_{max}) was highest in TDCIPP followed by TCEP and TCIPP (Figs. 3–5). C_{max} in the brain and adipose tissue was high for TCEP, TDCIPP and TCIPP respectively. Both the data and simulation results showed that OPFRs concentrations in all the organs declined by more than half of their C_{max} after 24 h of dosing (Figs. 3–5) except for brain and adipose tissue where this decline was very slow. Accumulation in TDCIPP was high (brain and adipose tissue) compared to the other two OPFRs at 168 h. The urinary elimination followed the following order: TCEP>TCIPP>TDCIPP whereas the feces elimination: TDCIPP>TCIPP>TCEP. In TCEP, feces elimination was less than 6%, so it was not included in the model.

The calibrated TDCIPP model was used to predict the concentration-time profile for different organs and compared with experimental data upon oral administration of 2 μg/Kg BW (Nomeir et al., 1981). The model was able to explain almost all time points (Fig. 6) (Fig S2 supp file). However, the chemical concentrations in kidney, urine, and feces are 1–2-fold outside the median model predictions, consistent with the World Health Organization PBK precision criterion (on Chemical Safety and for the Sound Management of Chemicals, 2010). In the case of urine, the experimental data was explained by a higher percentile (97.5) simulation and for feces, it was explained by 2.5 percentile. Another independent experimental dataset from Lynn et al. was compared with the simulated data for TDCIPP till 120 h (Fig. 7) (Lynn et al., 1981). The model was able to explain the concentration-time profile for organs like plasma, liver, kidney, urine and feces. But the plot for brain and fat was not explained by this model (Fig. 8). In the case of urine, our model underpredicted but the simulated median was within three-fold of the experimental data. The model overpredicted the amount of cumulative feces but it was close to the 2.5 percentile (Fig. 7).

3.2. Goodness of fit

PBK Model was able to adequately describe the concentration-time

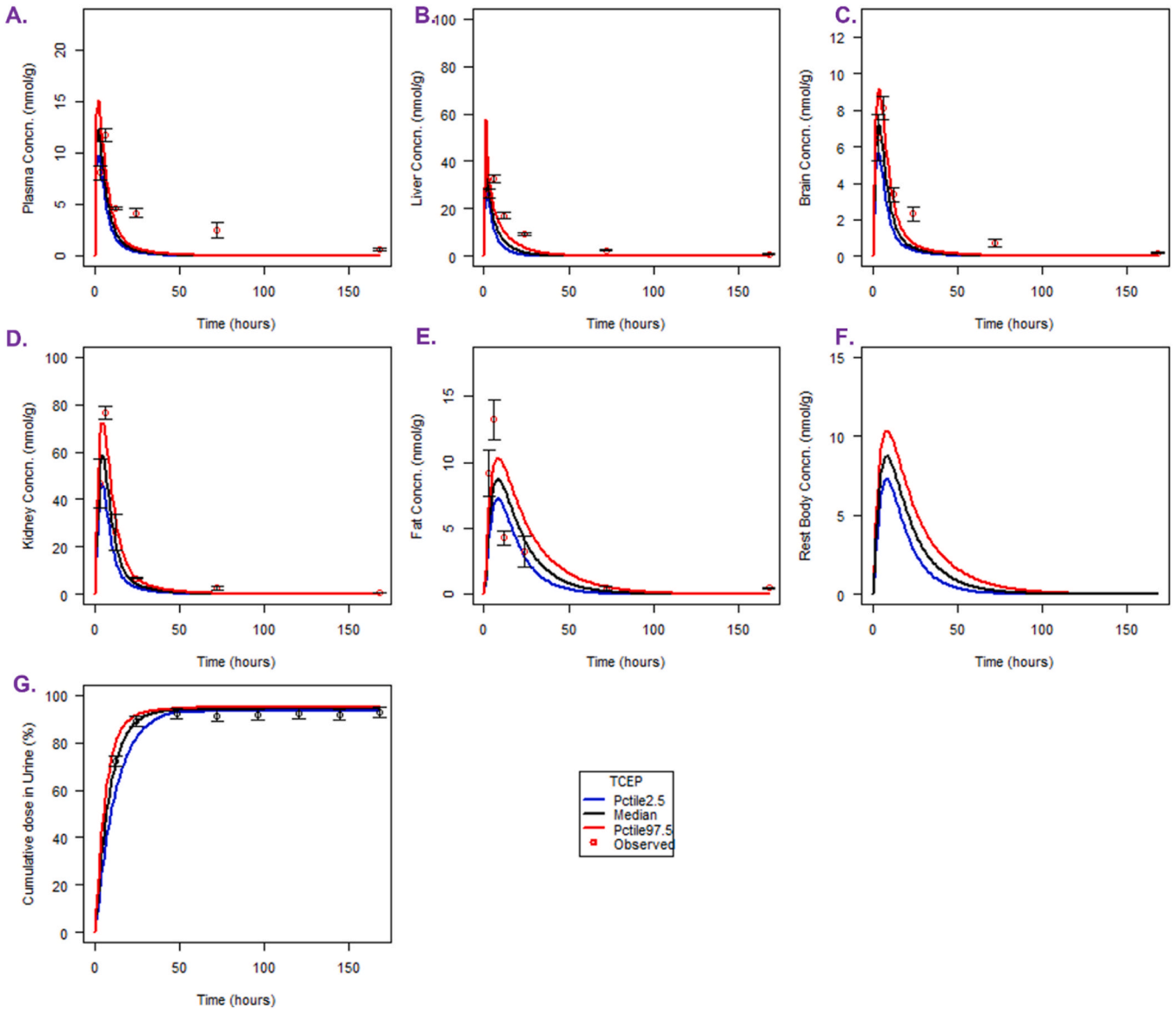

Fig. 5. Concentration-time curves for TCEP in plasma (A), liver (B), brain (C), kidney (D), fat (E), rest body (F), urine (G) at 50 μmol/Kg. The Y-axis showed the chemical concentrations (nmol/g) and cumulative dose excreted in urine and feces (%) and the X-axis showed the time in hrs. The solid lines correspond to the model simulation i.e., red (97.5th percentile), black (median), and blue (2.5th percentile), and the red dots (mean) with black bars (Standard deviations) represent the experimental value (Minegishi et al., 1988).

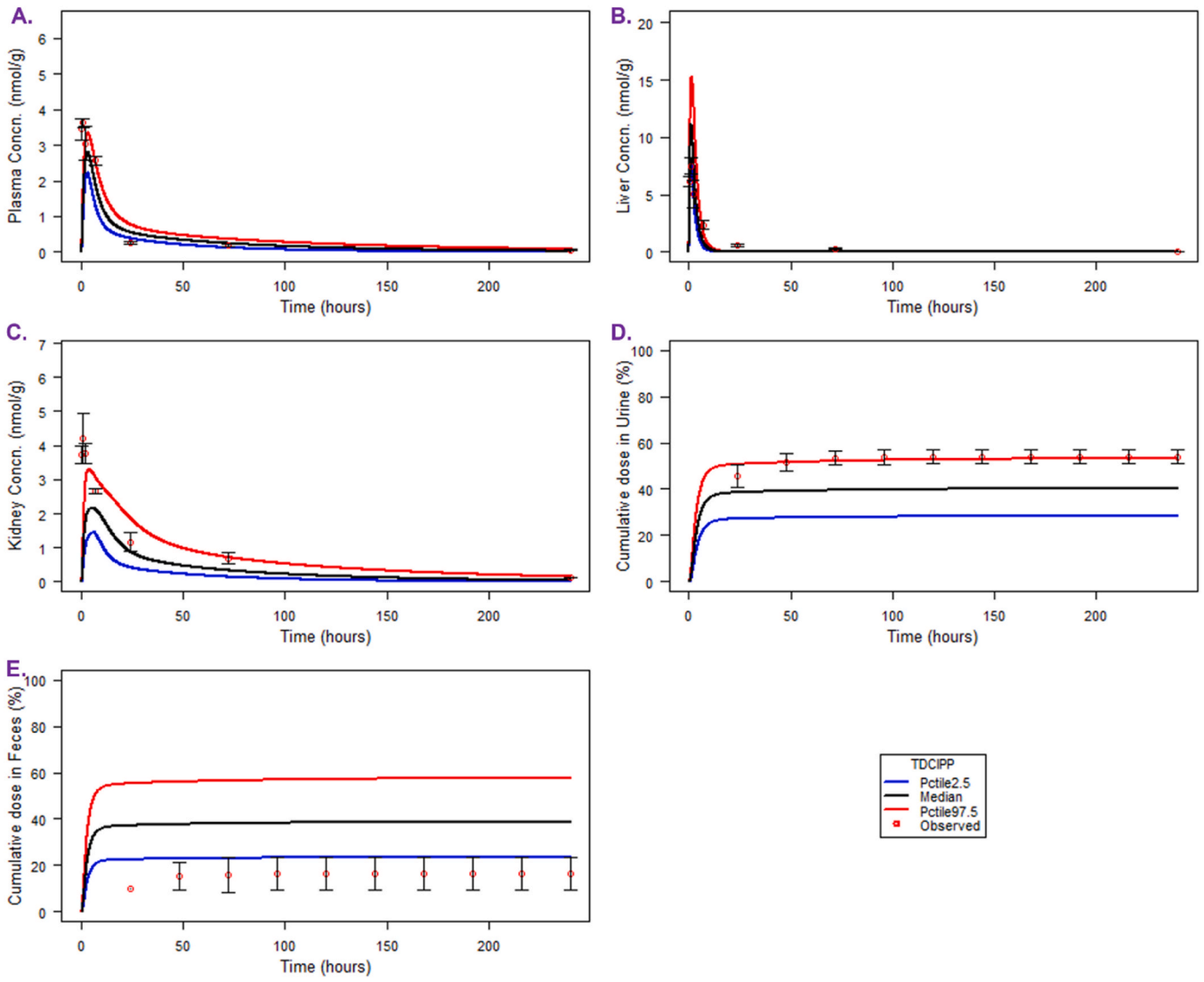

Fig. 6. Simulated vs experimental TDCIPP concentration-time curves of different organs i.e., plasma (A), liver (B), kidney (C), urine (D) and feces (E) at 2 μg/Kg BW. The Y-axis showed the chemical concentrations (nmol/g) and cumulative dose excreted in urine and feces (%) and the X-axis showed the time in hrs. The solid lines correspond to the model simulation i.e., red (97.5th percentile), black (median), and blue (2.5th percentile), and the red dots (mean) with black bars (Standard deviations) represent the experimental value (Nomeir et al., 1981).

profile for all organs as depicted by the goodness-of-fit plot. The correlation coefficient for all organs was above 0.7 based on PCC (Fig. 9, S3, S4). In Fig. 9, the correlation coefficient was above 0.95 for plasma, urine and feces for TDCIPP. For other organs, correlation coefficient was 0.75–0.85. For TCIPP, the correlation coefficient was above 0.9 for all the organs except the brain and feces where it was above 0.8 (Fig S3). Fig S4 represents the correlation coefficient for TCEP, and it was above 0.8 for all organs except fat where it was 0.78.

3.3. Sensitivity analysis

Local SA was performed for all the parameters used for developing PBK and the result has been summarized in Fig S5-S7. As expected, plasma AUC is having negative correlation towards renal clearance (Cl) in the case of all three compounds, however, the degree of sensitivity varies. A decrease in renal clearance will lead to an increase in plasma AUC as more compound will be getting circulated in the body. EHR had a higher negative effect for TDCIPP and TCIPP (Fig S5, S6) but for TCEP, the sensitivity was relatively low (Fig S7). A similar negative trend was followed by liver: plasma partition coefficient but more sensitivity towards TCEP. Later finding suggest that decreasing the EHR rate and liver blood flow means more plasma levels as less compounds will be distributed in the liver and gut, thus less fecal elimination. Interestingly, metabolic rate constant (K_{mliver_bcipp}) and body weight (BW) has a positive correlation with the plasma levels. In the case of TCIPP, body weight has a profound positive effect on the plasma followed by a negative effect from K_liver_plasma and Cl (Fig S6) similar to TDCIPP. TCEP also show the same pattern towards BW, K_liver_plasma and Cl. Surprisingly, for TCEP fu has major impact than other parameters (Fig S7). Decreasing the fu leads to an increase in plasma concentration. Vmax (positive) and Km (negative) has the opposite impact for all OPFRs. It suggests that the distribution of both these parameters could improve the plasma concentration profile. Figures for GSA have been provided in supplementary file 2 (Fig S8-S10).

3.4. Application of PBK model in neurotoxicity

A reverse dosimetry approach (Dosimetry IVIVE) was used to calculate the oral equivalent exposure utilizing a developed PBK model (Table 2). The exposure with toxic effect was considered for the maximum brain concentration (C_{max}) and then MCMC was used for calculating OED for TDCIPP and TCEP. All potential scale reduction

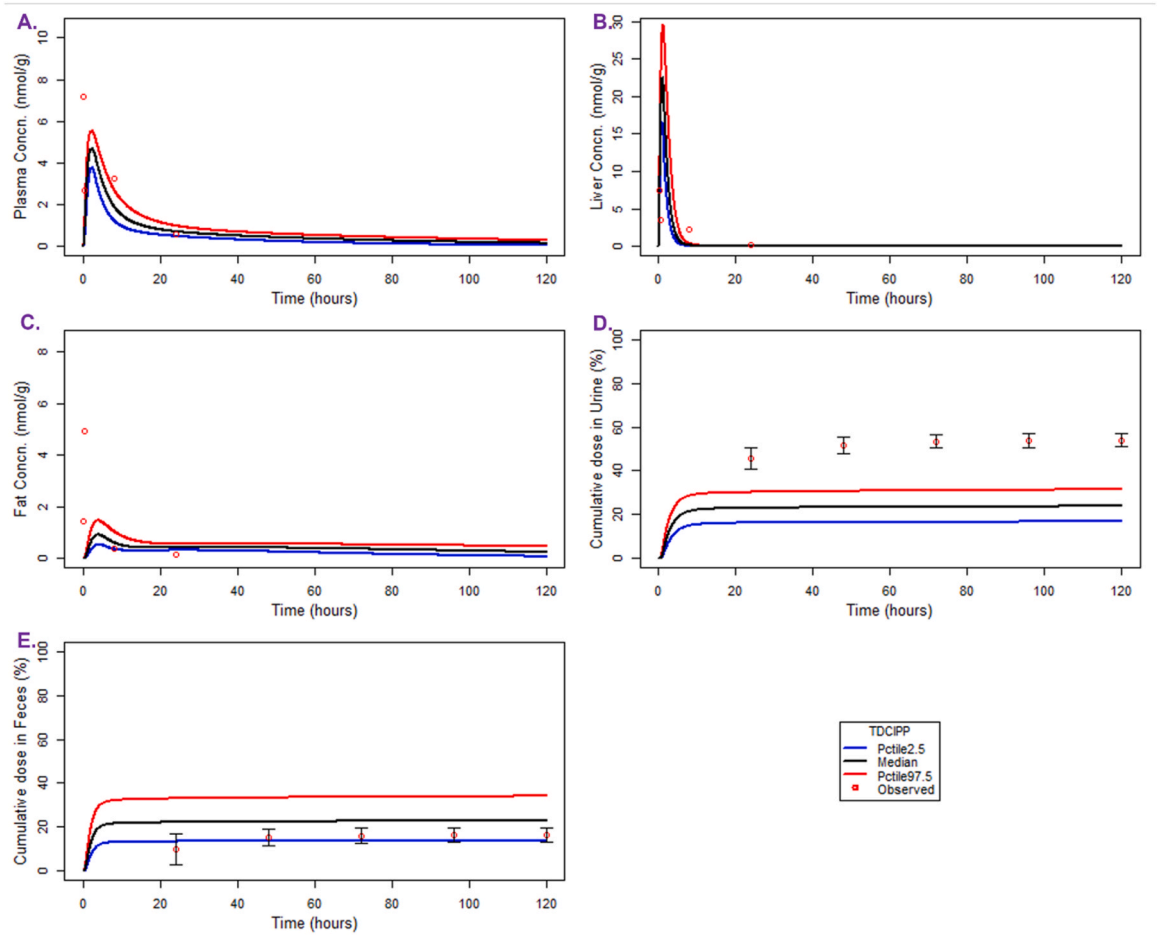

Fig. 7. Concentration-time curves for TDCIPP of plasma (A), liver (B), kidney (C), urine (D) and feces (E) at 10.04 μCi, sp. act. 12.5 mCi/mmol. The Y-axis showed the chemical concentrations (nmol/g) and cumulative dose excreted in urine and feces (%) and the X-axis showed the time in hrs. The solid lines correspond to the model simulation i.e., red (97.5th percentile), black (median), and blue (2.5th percentile), and the red dots (mean) with black bars (Standard deviations) represent the experimental value (Lynn et al., 1981).

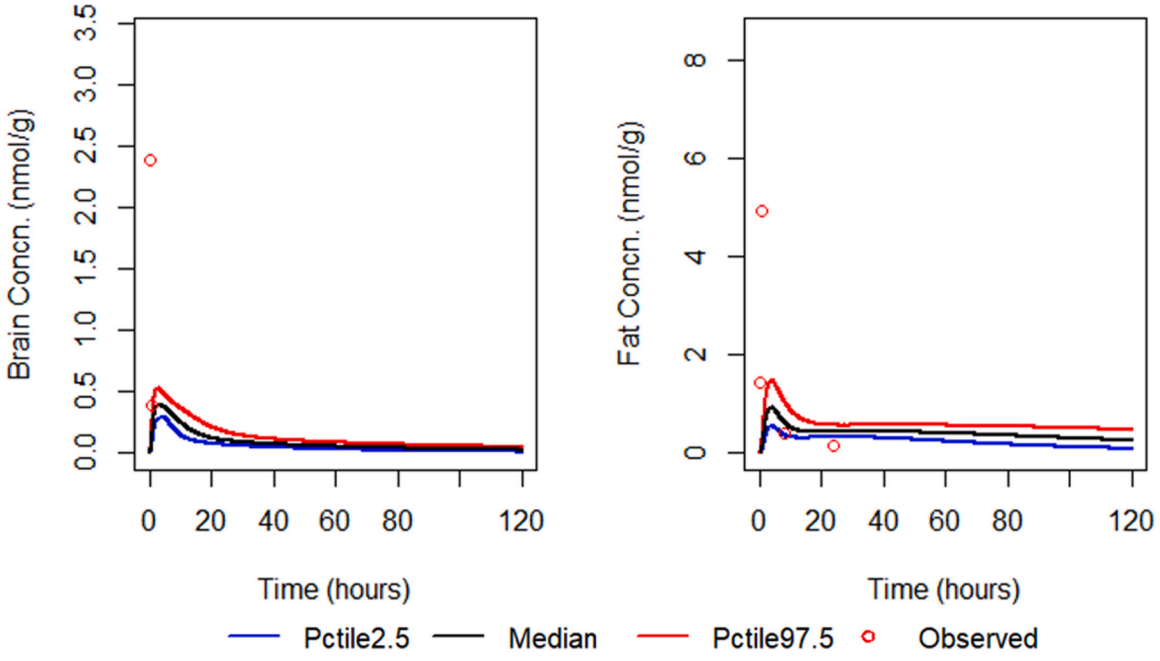

Fig. 8. Concentration-time plot for brain and fat with simulated and experimental data from Lynn et al. for TDCIPP at 10.04 μCi, sp. act. 12.5 mCi/mmol (Lynn et al., 1981). Blue line represents percentile 2.5, black line represents median and red line represents percentile 97.5 and red circle represents observed (experimental) data.

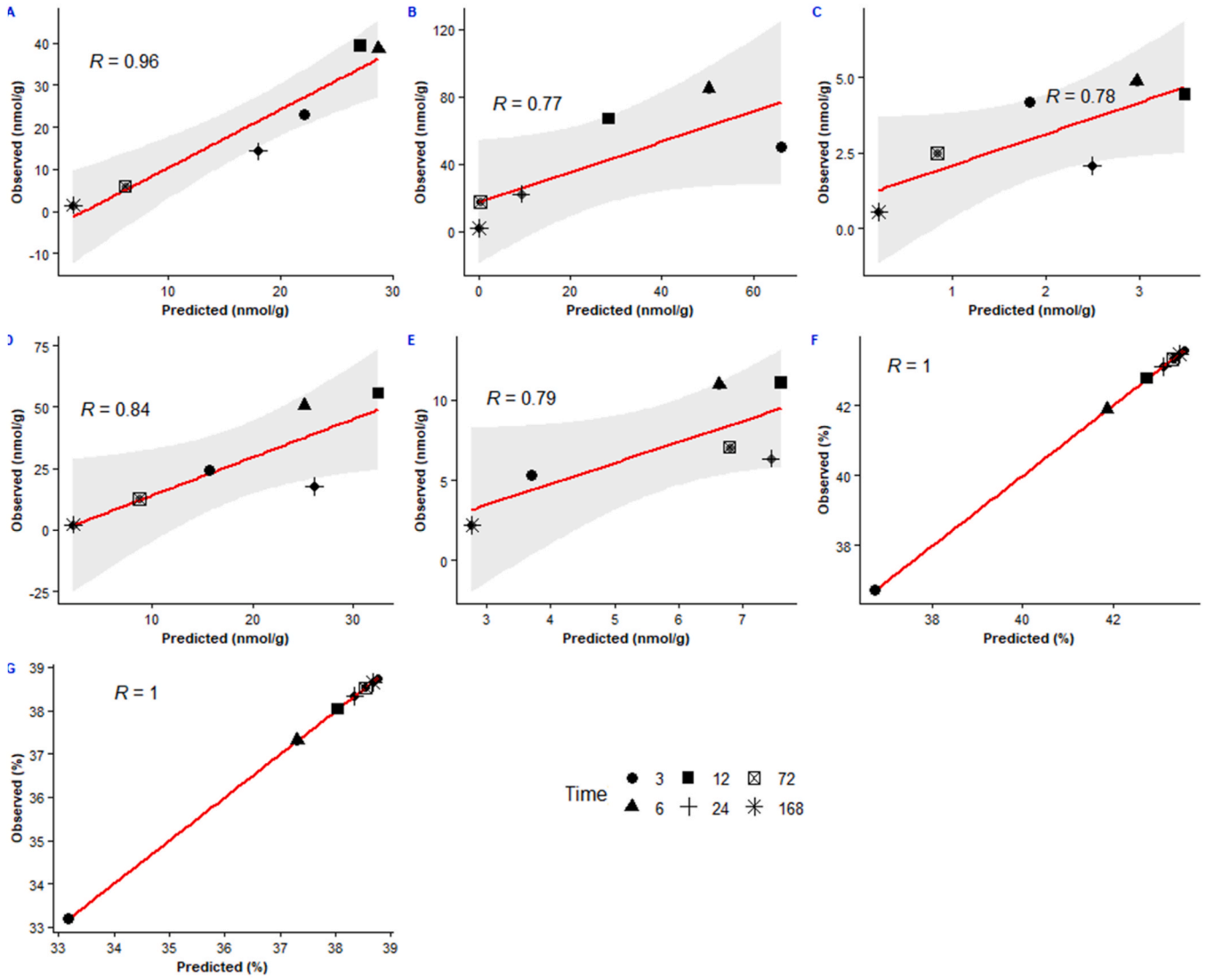

Fig. 9. Goodness-of-fit plot for TDCIPP for several organs at various time point till 168 h taking simulation and experimental data at 50 μmol/Kg (Minegishi et al., 1988). R (correlation coefficient) was above 70% for all the organs using Pearson correlation coefficient (PCC). Red line indicates the 50th percentile and grey band indicates the 95% confidence interval. A represents plasma, B: Liver, C: Brain, D: Kidney, E: Fat, F: Urine and G: Feces.

Table 2
Dosing for in-vitro study using PC12 cell line and reconstructed exposure for in-vivo.

Chemical	Exposure for OED (μM)	Cell-line	Reconstructed exposure using dosimetry IVIVE (mmol/Kg)	Reference
TDCIPP	50	PC12	40.5754	(Li et al., 2017a)
TDCIPP	50	PC12	40.5754	(Ta et al., 2014)
TCEP	200	PC12	3.893	(Ta et al., 2014)

factor (R) values were below 1.2 and Markov chain trace plots (Fig S11, S12 in supplementary file) further added confidence for the convergence among the chains for reverse dosimetry. The PBK model estimated a dose of 40.5754 mmol/Kg BW for TDCIPP (Li et al., 2017a). OED was found to be 3.893 mmol/Kg BW for TCEP to get the estimated brain concentration of 200 μM respectively and cause neuronal toxicity (Ta et al., 2014).

4. Discussion

For evaluating the pharmacokinetics of chemicals in various organs and tissues, the PBK model serves as a valuable tool. They can be used to comprehend the relationship between external exposure and its effect on the body. In this paper, a PBK Model for rats was developed to gain insight into the tissue disposition properties of three OPFRs. The data by Minegishi et al. was used to optimize the model parameters and later to check the predictability of the model (1988). Two independent datasets were used to further evaluate the model performance (Nomeir et al., 1981, Lynn et al., 1981). The uncertainty was included in the model for biochemical parameters to capture the observed concentration within predicted intervals. As per a commonly applied criterion for PBK, the observed and predicted concentration can be within two folds for general compounds (Shebley et al., 2018) which was observed in our model with data from Minegishi et al. (1988).

The disposition of all three OPFRs was quite extensive in the liver and kidney both being the metabolizing and elimination sites. In contrast, the concentration in the brain was lower than all other organs but still, a good quantity of OPFRs was detected in the brain (TCEP>TDCIPP>TCIPP, based on C_{max}). All of these molecules follow

Lipinski rule of five; a molecular weight less than 500 (TDCIPP: 430.5, TCIPP: 327.6, TCEP: 285.5 g/mol), log P less than 5 (3.65, 2.6, 1.43), hydrogen bond donor 0 (all OPFRs), and hydrogen bond acceptor less than 10 (4 for all), making them a good candidate for permeating the blood-brain-barrier (Neidle, 2012). Another major point was that rather than influx, efflux from the brain was quite slow (can be inferred based on the elimination phase of the concentration-time course) for all three OPFRs. There can be a possibility that these compounds bind with specific proteins inside the brain tissue extensively. For instance, a study by Kavass et al. showed that relative tissue binding (brain and plasma) knowledge is required for compounds to evaluate the active transport that affects CNS exposure (Cory Kalvass and Maurer, 2002). But, for OPFRs, we don't have such experimental data available in the literature. However, a zebrafish study showed that the slow efflux of OPFRs might be responsible for their neurotoxic effect. For instance, Li et al. demonstrated that exposure to TDCIPP potentially down-regulate the expression of neurodevelopmental genes and protein biomarkers (α-1 tubulin, syn 2a, mbp etc.) in zebrafish larvae (Li et al., 2018) leading to neurotoxicity. Additionally, it was observed that these compounds metabolize very fast inside the rat, and further mechanistic pathways for the neurotoxic potential of metabolites need to be investigated.

Another key point from the simulation was that all OPFRs' residence time is longer in the adipose tissue than in all other organs. This can be implicated partially to the lipophilicity of these chemicals. However, our model was not able to explain the last time point and adjusting the partition coefficient for adipose tissue did not result in a good fit (data not shown). Dobrev et al. (2003) explained this kind of phenomenon with hexamethyldisiloxane, a class of FRs, which accumulated inside lipoprotein and deep fat, acting as a reservoir. Compounds like chlorodecane (CDC) and dichlorophenyltrichloroethane (DDT) also showed similar trends with lymphatic and lipoprotein sequestration (Soine et al., 1982). Being chemical congeners, it is highly likely that OPFRs would also follow a similar mechanism. Further addition of deep adipose tissue as a sub-compartment might lead to improvement in the model fitting. We did not find enough data in the literature regarding lipoprotein sequestration for these compounds, hence this was not included in the model.

In the case of two independent data sets for TDCIPP, the model was able to explain certain organs like plasma, and kidney, but not brain and adipose tissue. The point worth mentioning is that the model has been optimized for higher doses, however, for extremely lower doses, an additional rate constant or other mechanism might need to be introduced. Another reason might be that the influx rate for adipose and brain in case of extremely low dose can be higher or the inclusion of influx and efflux rate can better explain. The model is underestimating the concentration by 3–4-fold only at the starting time points, at later time points the model is able to explain the kinetics. But further data is required to understand the reason behind this. In urine, our model showed a little underprediction while in feces it was overprediction for independent datasets, but the data was within three folds. The reason behind this could be the drastic variation in EHR rate with dose which may affect the concentration in plasma and hence the excretion but due to a deficiency of data, it is not possible to evaluate such scenarios and include further parameters in the PBK model. Another possibility can be an introduction of permeability-limited compartments for organs like adipose and brain, so further improvement in the model can be integrating perfusion-limited PBK with permeability limited for specific organs. Local and Global Sensitivity analysis performed for the PBK model was based on a 2% change in the physiological and biochemical parameters after a single dose exposure and measuring the plasma AUC till 168-hour post-exposure. Physiological parameter like body weight and blood flow to the liver from plasma is highly related to variation in AUC suggesting the importance of physiological parameters. Regarding biochemical parameters, clearance (urine elimination rate constant) and fu has a major impact on plasma AUC.

Pharmacokinetic models with IVIVE have a big application in the field of toxicokinetics for estimating doses. Here, we showed the case studies considering TDCIPP and TCEP only, since we could not find any relevant in-vitro study related to neurotoxicity for TCIPP. The brain was considered as a target organ since the recent epidemiological and in-vitro studies are pointing towards a possible neurotoxicity of OPFRs (Blum et al., 2019; Sugeng et al., 2021; Sun et al., 2016). Two in-vitro studies were considered to calculate OED with the highest in-vitro dose as input. The first study by Ta et al. considered undifferentiated PC-12 rat pheochromocytome cell lines as a model to evaluate viability, apoptosis and morphology caused by exposure to TDCIPP and TCEP. At 200 μM and 50 μM TCEP and TDCIPP respectively, neurotoxicity was observed through nerve fibre damage, nerve node reduction, and effect on synaptogenesis and neurite outgrowth. A second study by Li et al. also used similar PC-12 cell lines to understand cytotoxicity induced after exposure to TDCIPP for 4 days. Authors have found that TDCIPP-induced toxicity could be due to increased calcium levels, increased CAMK2 phosphorylation and activation of p38 MAPK, ERK1/2 and JNK pathways many of which were found to be activated at 50 μM. Further information about these cell lines can be referred to literature (Li et al., 2017a; Ta et al., 2014). Two concentrations i.e., 50 (TDCIPP) and 200 μM (TCEP) were used at which in-vitro toxicity was observed and converted to biological concentration considering the living being ADME profile. It seems that a very high concentration of TDCIPP and TCEP is required to produce neuronal adverse effects in animals as per in-vitro reverse dosimetry. The equivalent in-vivo dose can be used by experimental researchers to evaluate the neurotoxicity in rats. There is some research showing that these compounds may have a neurotoxic effect due to their structural similarity with organophosphorus pesticides (Dishaw et al., 2014). However, further experimental studies are required to evaluate their neurotoxic potential in rats. Considering the limited data available for the evaluation of the model by OPFRs, there can be some uncertainty in the predicted OED. But, there remains a scope to improve the PBK model in future, especially for the brain region by including a permeability rate constant for the brain based on experimental in-vitro or in-vivo data.

5. Conclusion and future outlook

PBK models are currently used for exposure, kinetics, inter-species and toxicological risk assessment. The current model serves as an important starting point for extrapolation to other species and understanding the toxicokinetics in human beings. The developed PBK model was evaluated at several doses where experimental data were available. For instance, the model was able to explain the kinetics data, showing the model reliability. The metabolite has been included and major compartments of living beings were taken extending the usage of this model to understand the kinetics of OPFRs in several species. With the available literature data, we found that for higher doses, perfusion limited kinetic model can explain the concentration-time profile in rats, however, at low doses the PBK model was not able to explain the disposition in two organs. To improve this, permeation limited approach can be applied for brain and adipose tissue. Also, we showed the dosimetry IVIVE application of this model by extrapolating in-vitro data to equivalent in-vivo exposure in the field of neurotoxicity which can be used further to evaluate toxic effect of these chemicals on central nervous system or neurodevelopment. This model serves as a framework to understand the ADME profile for OPFRs and also focuses on the perspective that sometimes alone perfusion limited PBK is not enough. Further, this model can be extrapolated to predict the OPFRs kinetics in humans as a prototype model and can be optimized on the availability of experimental data in the near future. This can be used for reconstructed exposure based on urine or plasma data to understand how much human population is being exposed on a daily basis by OPFRs via several exposure routes. Some of the important understanding from this model is the slow efflux from the brain, OPFRs getting accumulated in adipose tissue for a longer time and the role of EHR in explaining the longer half-

life in rats.

CRediT authorship contribution statement

D. Deepika: Methodology, Investigation, Writing – original draft. **R. P. Sharma**: Methodology, Review and Supervision; **M. Schuhmacher**: Funding acquisition, Review and Supervision; and **Vikas Kumar**: Funding acquisition, Methodology, Review and Supervision.

Declaration of Competing Interest

The authors declare the following financial interests/personal relationships which may be considered as potential competing interests: Vikas Kumar reports financial support was provided by European Commission. Marta Schuhmacher reports was provided by European Commission. Marta Schuhmacher reports financial support was provided by Spanish Ministry of Science, Innovation and Universities.

Data availability

No data was used for the research described in the article.

Acknowledgments

This study was financially supported by the European Union Marie Skłodowska-Curie "Neurosome project" under grant agreement no. 766251, co-funded project European Partnership for the Assessment of Risks from Chemicals (PARC) under Grant Agreement No 101057014 and FlameRisk project under grant agreement number RTI2018-095466-B-I00 funded by the Spanish Ministry of Science, Innovation and Universities. This publication reflects only the author views. The community and other funding organizations are not liable for any use made of the information contained.

Appendix A. Supporting information

Supplementary data associated with this article can be found in the online version at doi:10.1016/j.toxlet.2023.06.006.

References

Bajard, L., Melymuk, L., Blaha, L., 2019. Prioritization of hazards of novel flame retardants using the mechanistic toxicology information from ToxCast and Adverse Outcome Pathways. Environ. Sci. Eur. 31, 14. https://doi.org/10.1186/s12302-019-0195-z.

Blum, A., Behl, M., Birnbaum, L.S., Diamond, M.L., Phillips, A., Singla, V., Sipes, N.S., Stapleton, H.M., Venier, M., 2019. Organophosphate ester flame retardants: are they a regrettable substitution for polybrominated diphenyl ethers? Environ. Sci. Technol. Lett. 6, 638–649. https://doi.org/10.1021/acs.estlett.9b00582.

Bois, F.Y., 2009. GNU MCSim: Bayesian statistical inference for SBML-coded systems biology models. Bioinformatics 25, 1453–1454. https://doi.org/10.1093/bioinformatics/btp162.

Brown, R.P., Delp, M.D., Lindstedt, S.L., Rhomberg, L.R., Beliles, R.P., 1997. Physiological parameter values for physiologically based pharmacokinetic models. Toxicol. Ind. Health 13, 407–484. https://doi.org/10.1177/074823379701300401.

Chapman, D.E., Michener, S.R., Powis, G., 1991. Metabolism of the flame retardant plasticizer tris(2-chloroethyl) phosphate by human and rat liver preparations. Toxicol. Sci. 17, 215–224. https://doi.org/10.1093/toxsci/17.2.215.

Chupeau, Z., Bonvallot, N., Mercier, F., le Bot, B., Chevrier, C., Glorennec, P., 2020. Organophosphorus flame retardants: a global review of indoor contamination and human exposure in europe and epidemiological evidence. Int J. Environ. Res Public Health 17, 6713. https://doi.org/10.3390/ijerph17186713.

Cory Kalvass, J., Maurer, T.S., 2002. Influence of nonspecific brain and plasma binding on CNS exposure: implications for rational drug discovery. Biopharm. Drug Dispos. 23, 327–338. https://doi.org/10.1002/bdd.325.

Dishaw, L. v, Hunter, D.L., Padnos, B., Padilla, S., Stapleton, H.M., 2014. Developmental exposure to organophosphate flame retardants elicits overt toxicity and alters behavior in early life stage zebrafish (danio rerio. Toxicol. Sci. 142, 445–454. https://doi.org/10.1093/toxsci/kfu194.

Dobrev, I.D., Reddy, M.B., Plotzke, K.P., Varaprath, S., McNett, D.A., Durham, J., Andersen, M.E., 2003. Closed-chamber inhalation pharmacokinetic studies with hexamethyldisiloxane in the rat. Inhal. Toxicol. 15, 589–617. https://doi.org/10.1080/08958370390205083.

Emond, C., DeVito, M.J., Birnbaum, L.S., 2021. A PBPK model describing the pharmacokinetics of γ-HBCD exposure in mice. Toxicol. Appl. Pharm. 428, 115678 https://doi.org/10.1016/j.taap.2021.115678.

Esplugas, R., Rovira, J., Mari, M., Fernández-Arribas, J., Eljarrat, E., Domingo, J.L., Schuhmacher, M., 2022. Emerging and legacy flame retardants in indoor air and dust samples of Tarragona Province (Catalonia, Spain. Sci. Total Environ. 806, 150494 https://doi.org/10.1016/j.scitotenv.2021.150494.

Hoffman, K., Daniels, J.L., Stapleton, H.M., 2014. Urinary metabolites of organophosphate flame retardants and their variability in pregnant women. Environ. Int 63, 169–172. https://doi.org/10.1016/j.envint.2013.11.013.

Hogberg, H.T., de Cássia da Silveira, E., Sá, R., Kleensang, A., Bouhifd, M., Cemiloglu Ulker, O., Smirnova, L., Behl, M., Maertens, A., Zhao, L., Hartung, T., 2021. Organophosphorus flame retardants are developmental neurotoxicants in a rat primary brainsphere in vitro model. Arch. Toxicol. 95, 207–228. https://doi.org/10.1007/s00204-020-02903-2.

Hou, R., Xu, Y., Wang, Z., 2016. Review of OPFRs in animals and humans: Absorption, bioaccumulation, metabolism, and internal exposure research. Chemosphere 153, 78–90. https://doi.org/10.1016/j.chemosphere.2016.03.003.

Hsieh, N.-H., Reisfeld, B., Chiu, W.A., 2020. pksensi: An R package to apply global sensitivity analysis in physiologically based kinetic modeling. SoftwareX 12, 100609. https://doi.org/10.1016/j.softx.2020.100609.

Huang, J., Ye, L., Fang, M., Su, G., 2022. Industrial production of organophosphate flame retardants (OPFRs): big knowledge gaps need to be filled? Bull. Environ. Contam. Toxicol. 108, 809–818. https://doi.org/10.1007/s00128-021-03454-7.

Ingle, M.E., Mínguez-Alarcón, L., Carignan, C.C., Butt, C.M., Stapleton, H.M., Williams, P. L., Ford, J.B., Hauser, R., Meeker, J.D., 2018. The association between urinary concentrations of phosphorous-containing flame retardant metabolites and semen parameters among men from a fertility clinic. Int J. Hyg. Environ. Health 221, 809–815. https://doi.org/10.1016/j.ijheh.2018.05.001.

Li, C., Li, L., Lin, B., Fang, Y., Yang, H., Liu, H., Xi, Z., 2017. Tris (1,3-dichloro-2-propyl) phosphate induces toxicity by stimulating CaMK2 in PC12 cells. Environ. Toxicol. 32, 1784–1791. https://doi.org/10.1002/tox.22401.

Li, R., Wang, H., Mi, C., Feng, C., Zhang, L., Yang, L., Zhou, B., 2019. The adverse effect of TCIPP and TCEP on neurodevelopment of zebrafish embryos/larvae. Chemosphere 220, 811–817. https://doi.org/10.1016/j.chemosphere.2018.12.198.

Li, R., Zhang, L., Shi, Q., Guo, Y., Zhang, W., Zhou, B., 2018. A protective role of autophagy in TDCIPP-induced developmental neurotoxicity in zebrafish larvae. Aquat. Toxicol. 199, 46–54. https://doi.org/10.1016/j.aquatox.2018.03.016.

Loccisano, A.E., Longnecker, M.P., Campbell, J.L., Andersen, M.E., Clewell, H.J., 2013. Development of pbpk models for pfoa and pfos for human pregnancy and lactation life stages. J. Toxicol. Environ. Health (Issues 76), 25–57. https://doi.org/10.1080/15287394.2012.722523.

Lynn, R.K., Wong, K., Garvie-Gould, C., Kennish, J.M., 1981. Disposition of the flame retardant, tris(1,3-dichloro-2-propyl) phosphate, in the rat. Drug Metab. Dispos. 9, 434–441.

McNally, K., Sams, C., Hogg, A., Lumen, A., Loizou, G., 2021. Development, testing, parameterisation and calibration of a human PBPK model for the plasticiser, Di-(2-propylheptyl) Phthalate (DPHP) using in silico, in vitro and human biomonitoring data. Front Pharmacol. 12. https://doi.org/10.3389/fphar.2021.692442.

Merrill, E.A., Clewell, R.A., Gearhart, J.M., Robinson, P.J., Sterner, T.R., Yu, K.O., Mattie, D.R., Fisher, J.W., 2003. PBPK predictions of perchlorate distribution and its effect on thyroid uptake of radioiodide in the male rat. Toxicol. Sci. 73, 256–269. https://doi.org/10.1093/toxsci/kfg080.

Minegishi, K., Kurebayashi, H., Nambaru, S., Morimoto, K., Takahashi, T., Yamaha, T., 1988. Comparative studies on absorption, distribution, and excretion of flame retardants halogenated alkyl phosphate in rats. Eisei kagaku 34, 102–114. https://doi.org/10.1248/jhs1956.34.102.

Neidle, S., 2012. Design principles for quadruplex-binding small molecules. In: Neidle, S. (Ed.), Therapeutic Applications of Quadruplex Nucleic Acids. Elsevier, Boston, pp. 151–174. https://doi.org/10.1016/B978-0-12-375138-6.00009-1.

Nomeir, A.A., Kato, S., Matthews, H.B., 1981. The metabolism and disposition of tris(1,3-dichloro-2-propyl) phosphate (fyrol FR-2) in the rat. Toxicol. Appl. Pharm. 57, 401–413. https://doi.org/10.1016/0041-008X(81)90238-6.

on Chemical Safety, I.P., for the Sound Management of Chemicals, I.-O.P., 2010. Characterization and application of physiologically based phamacokinetic models in risk assessment. IPCS harmonization project document; no. 9.

Poma, G., Glynn, A., Malarvannan, G., Covaci, A., Darnerud, P.O., 2017. Dietary intake of phosphorus flame retardants (PFRs) using Swedish food market basket estimations. Food Chem. Toxicol. 100, 1–7. https://doi.org/10.1016/j.fct.2016.12.011.

Schreder, E., 2019. Europe bans most harmful class of flame retardants in TVs [WWW Document]. Safer Chemicals, Healthy Families. URL ⟨https://saferchemicals.org/2019/10/01/europe-bans-most-harmful-class-of-flame-retardants-in-tvs/⟩.

Sharma, R.P., Kumar, V., Schuhmacher, M., Kolodkin, A., Westerhoff, H. v, 2020. Development and evaluation of a harmonized whole body physiologically based pharmacokinetic (PBPK) model for flutamide in rats and its extrapolation to humans. Environ. Res (182), 108948. https://doi.org/10.1016/j.envres.2019.108948.

Shebley, M., Sandhu, P., Emami Riedmaier, A., Jamei, M., Narayanan, R., Patel, A., Peters, S.A., Reddy, V.P., Zheng, M., de Zwart, L., Beneton, M., Bouzom, F., Chen, J., Chen, Y., Cleary, Y., Collins, C., Dickinson, G.L., Djebli, N., Einolf, H.J., Gardner, I., Huth, F., Kazmi, F., Khalil, F., Lin, J., Odinecs, A., Patel, C., Rong, H., Schuck, E., Sharma, P., Wu, S.-P., Xu, Y., Yamazaki, S., Yoshida, K., Rowland, M., 2018. Physiologically based pharmacokinetic model qualification and reporting procedures for regulatory submissions: a consortium perspective. Clin. Pharm. Ther. 104, 88–110. https://doi.org/10.1002/cpt.1013.

Soine, P.J., Blanke, R. v, Guzelian, P.S., Schwartz, C.C., 1982. Preferential binding of chlordecone to the protein and high density lipoprotein fractions of plasma from humans and other species. J. Toxicol. Environ. Health 9, 107–118. https://doi.org/10.1080/15287398209530146.

Sugeng, E.J., de Cock, M., Leonards, P.E.G., Bor, M. van de, 2021. Association of exposure to organophosphate flame retardants and children's behavior at a median age of 18 months. Environ. Adv. 5, 100077 https://doi.org/10.1016/j.envadv.2021.100077.

Sun, L., Tan, H., Peng, T., Wang, S., Xu, W., Qian, H., Jin, Y., Fu, Z., 2016. Developmental neurotoxicity of organophosphate flame retardants in early life stages of Japanese medaka (Oryzias latipes). Environ. Toxicol. Chem. 35, 2931–2940. https://doi.org/10.1002/etc.3477.

Ta, N., Li, C., Fang, Y., Liu, H., Lin, B., Jin, H., Tian, L., Zhang, H., Zhang, W., Xi, Z., 2014. Toxicity of TDCPP and TCEP on PC12 cell: Changes in CAMKII, GAP43, tubulin and NF-H gene and protein levels. Toxicol. Lett. 227, 164–171. https://doi.org/10.1016/j.toxlet.2014.03.023.

Team, Rs., 2015. RStudio: Integrated Development Environment for R [Internet]. Boston, MA [WWW Document]. URL ⟨http://www.rstudio.com/⟩.

U. S. Environmental Protection Agency, 2006. Approaches for the Application of Physiologically Based Pharmacokinetic (PBPK) Models and Supporting Data in Risk Assessment, Epa/600/R-05/043F.

van den Eede, N., Maho, W., Erratico, C., Neels, H., Covaci, A., 2013. First insights in the metabolism of phosphate flame retardants and plasticizers using human liver fractions. Toxicol. Lett. 223, 9–15. https://doi.org/10.1016/j.toxlet.2013.08.012.

van den Eede, N., Tomy, G., Tao, F., Halldorson, T., Harrad, S., Neels, H., Covaci, A., 2016. Kinetics of tris (1-chloro-2-propyl) phosphate (TCIPP) metabolism in human liver microsomes and serum. Chemosphere 144, 1299–1305. https://doi.org/10.1016/j.chemosphere.2015.09.049.

Wang, C., Chen, Z., Lu, Y., Wang, L., Zhang, Y., Zhu, X., Song, J., 2020. Neurotoxicity and related mechanisms of flame retardant TCEP exposure in mice. Toxicol. Mech. Methods 30, 490–496. https://doi.org/10.1080/15376516.2020.1765060.

Wang, X., Shan, G., Zhu, L., 2020. Estimation of internal human daily intakes of organophosphate esters using one-compartment toxicokinetic model in the whole blood from Hebei Province, China. Environ. Res 186, 109493. https://doi.org/10.1016/j.envres.2020.109493.

Yang, J., Zhao, Y., Li, M., Du, M., Li, X., Li, Y., 2019. A review of a class of emerging contaminants: The classification, distribution, intensity of consumption, synthesis routes, environmental effects and expectation of pollution abatement to organophosphate flame retardants (opfrs). Int J. Mol. Sci. 20, 2874. https://doi.org/10.3390/ijms20122874.

Yang, Y., Chen, P., Ma, S., Lu, S., Yu, Y., An, T., 2022. A critical review of human internal exposure and the health risks of organophosphate ester flame retardants and their metabolites. Crit. Rev. Environ. Sci. Technol. 52, 1528–1560. https://doi.org/10.1080/10643389.2020.1859307.

Yao, C., Yang, H., Li, Y., 2021. A review on organophosphate flame retardants in the environment: Occurrence, accumulation, metabolism and toxicity. Sci. Total Environ. 795, 148837 https://doi.org/10.1016/j.scitotenv.2021.148837.

Zhang, X., Zou, W., Mu, L., Chen, Y., Ren, C., Hu, X., Zhou, Q., 2016. Rice ingestion is a major pathway for human exposure to organophosphate flame retardants (OPFRs) in China. J. Hazard Mater. 318, 686–693. https://doi.org/10.1016/j.jhazmat.2016.07.055.

Zhu, T., Zheng, X.-B., Yan, X., Tang, B., Zheng, J., Luo, X.-J., Zhu, C.-Y., Yu, Y.-J., Mai, B.-X., 2020. In vivo distribution and biotransformation of Tris (1,3-dichloro-2-propyl) phosphate in mice. Environ. Pollut. 263, 114595 https://doi.org/10.1016/j.envpol.2020.114595.